Numerical Modeling of 3-D Separated Flows at Reynolds Numbers Appropriate for Turbine Blades and Unmanned Aero Vehicles

By G. Castiglioni, J. A. Domaradzki, V. Pasquariello†, S. Hickel† AND M. Grilli†

Department of Aerospace Engineering
University of Southern California
Los Angeles, CA 90089-1191, USA

Flow separation strongly affects flows for unmanned aerial vehicles (UAV), micro air vehicles (MAV) and turbomachinery. The unsteady effects of flow separation greatly influence blade/wing lift and drag thus performance of UAV's, and efficiency and robustness of turbomachinery because of its impact on high cycle fatigue (HCF). The Reynolds numbers for the aforementioned devices are usually low to moderate. Low Reynolds number separated flows have been successfully simulated using direct numerical simulations (DNS). However, the large computational cost of DNS makes this technique not practical for industrial applications. Reynolds averaged Navier-Stokes (RANS) techniques have been only partially able to predict some features of low Reynolds number separated flows so far, leaving Large Eddy Simulation (LES) as a primary candidate for fast and accurate prediction tool for such flows. In this report we investigate the ability of LES techniques to accurately predict the behavior of such flows at a computational cost reduced significantly from the cost of DNS. We have performed 2-D and 3-D simulations of a laminar separation bubble on a NACA-0012 airfoil at $Re_c = 5 \times 10^4$ at 5 degree of incidence with resolution reduced from that used in DNS. For the 2-D simulations the results to date show good predictions for the pressure coefficient C_p and the friction coefficient C_f but only when using dissipative numerical schemes. For the 3-D simulations the results show a good prediction of the separation point, but inaccurate predictions of the reattachment point.

1. Introduction

Reynolds numbers for flows in rotating machinery, for unmanned aerial vehicles (UAV), micro air vehicles (MAV), wind turbines, and propellers are usually low or moderate. Based on wing/blade chord they are typically less than 2×10^6 and often only on the order of a few $10^4 - 10^5$. By comparison, civilian aeroplanes are characterized by the Reynolds numbers ranging from few millions to 80×10^6 for the Boeing 747 at cruising velocity. There is a long history of research on high Reynolds number aerodynamics, driven by its importance in the aerospace industry, and there exist robust numerical tools for the prediction of lift and drag forces for streamlined bodies. The recent experimental investigations of low Reynolds number aerodynamics [1–3] reveal new features

† Lehrstuhl für Aerodynamik und Strömungsmechanik, Technische Universität München, Boltzmannstr. 15, 85748 Garching b. München

of such flows that complicate their prediction compared with high Reynolds number flows. Aerodynamics at moderate and low Reynolds numbers is less developed because of a unique physical difficulty: such flows are often dominated by the effects of flow separation. The flow separation can greatly influence lift and drag, and thus flight stability of UAV's, efficiency of wind turbines, and unsteadiness in turbine flows, which is instrumental in predicting high cycle fatigue (HCF) for turbomachinery components. In order to produce efficient designs or control schemes to reduce separation effects we need prediction tools for such flows. However, while there are experimental data on both the time-averaged lift and drag forces and the instantaneous flow fields over wings, the agreement between different experiments is often poor, indicating that the separation process can be sensitive to details of experimental setups.

The physical origin of the observed behavior is qualitatively well understood: it is caused by a sudden appearance of the laminar separation bubble that changes the flow pattern around a wing and thus its properties. The main features of the laminar separation bubble are illustrated in Fig. 1 taken from [4]. The attached laminar boundary layer developing on a wing is subjected to an adverse pressure gradient due to the wing curvature that causes it to separate. Immediately behind the separation point there is an effectively stagnant flow region, the so-called "dead air" region, followed by a reverse flow vortex. The interface between the separated flow moving away from the wing and the recirculating flow in the vicinity of the wing results in a shear layer with an inflectional mean velocity profile. This shear layer experiences Kelvin-Helmholtz instabilities, developing into turbulence, after generating first characteristic spanwise vortices. Further downstream the separated turbulent flow reattaches and gradually evolves into the classical turbulent boundary layer. The above picture emerges from numerous experimental investigations, e.g., [1–3], as well as from direct numerical simulations (DNS) results [4–9]. Note that despite the fact that the term "laminar" is used, the actual flow is a mixture of regions where the flow is laminar, transitional, non-equilibrium turbulent boundary layer, and an equilibrium turbulent boundary layer.

The agreement between experiments and computations is even harder to find, indicating potential difficulties in developing separation prediction tools. This is because the separation process, especially driven by an adverse pressure gradient as opposed to geometry, is essentially non-equilibrium and involves subtle interactions between viscous, advective, and pressure effects that can be captured only by the full Navier-Stokes equations. Indeed, at present the reliable numerical results for such flows have to be obtained using DNS. However, such DNS require substantial computational resources, long wall-clock runs and long analysis times, e.g., [6] used over 170 million grid points for a relatively simple 3-D configuration. Such numerical simulations of the full Navier-Stokes equations are not feasible if a number of configurations and angles of attack are to be investigated. Therefore, other simulation options must be considered. One option is to employ Reynolds Averaged Navier-Stokes (RANS) models, modified to account for the reduction of the eddy viscosity around the separation region. This approach is commonly used and optimized for high Reynolds number turbulent flows, but not as useful for the separated flows of interest. Another option is to employ Large Eddy Simulation (LES) techniques. For instance, Yang and Voke [10] reported LES results obtained with the dynamic Smagorinsky model in a good agreement with experiments for boundary-layer separation and transition caused by surface curvature at $Re = 3,450$. Yet even for this relatively low Reynolds number, the critical issues in getting the agreement was good numerical resolution (472x72x64 mesh points) and a high order numerical

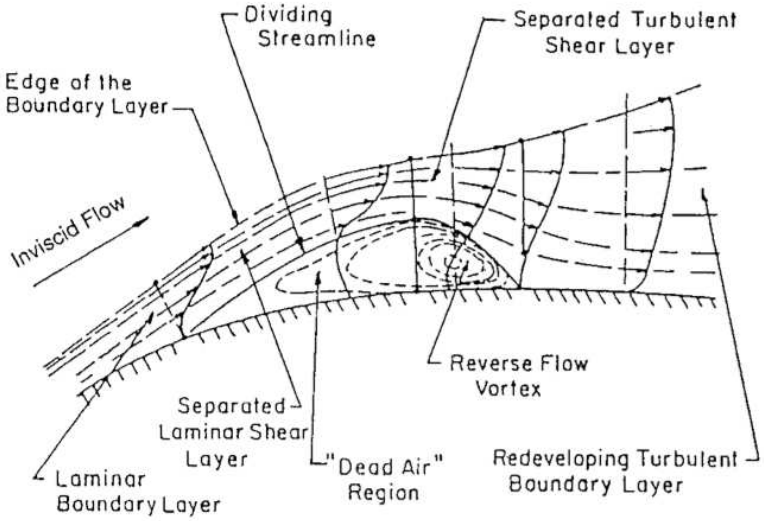

FIGURE 1. Features of a laminar separation bubble flow (after [4]).

method, requirements difficult to satisfy in simulations of practical flows often performed with low order finite difference or finite volume methods (e.g., commercial codes). Similarly, Eisenbach and Friedrich [11] performed LES of flow separation on an airfoil at high angle of attack at $Re = 10^5$ using Cartesian grids. This case also required very high resolutions between 50 and 100 million mesh points. A rare example of low resolution LES is given by Almutairi *et al.* [20]. In that study the results for a laminar separation bubble over an airfoil are in good agreement with [6, 7] at 4.5% of DNS resolution.

In the present report we study the same configuration: i.e., a separation problem for a flow around a wing/blade geometry at moderate Reynolds numbers using LES. The specific geometrical setting is that of a 3-D airfoil at incidence for which detailed DNS results were obtained in [6, 7]. The goal of the project is to reproduce the laminar separation bubble on a NACA-0012 airfoil at $Re_c = 5 \times 10^4$ at 5 degree of incidence with *resolution reduced drastically from that used in DNS and typical LES performed for this problem*. The reduction target is a factor of 100. To simulate this case the code INCA developed at TUM that uses immersed boundary method (IB) has been employed. Several simulations in 2-D and 3-D have been performed with varying resolution. In the attempt to match the DNS results for the 2-D case, simulations with 5 different numerical schemes have been done.

2. Numerical method

2.1. *Governing equations*

The numerical code solves the compressible three-dimensional Navier-Stokes equations in conservative form

$$\int_V \left(\frac{\partial \mathbf{U}}{\partial t} + \nabla \cdot [\mathbf{F}(\mathbf{U}) + \mathbf{G}(\mathbf{U})] \right) dV = 0 \,. \tag{2.1}$$

The solution vector $\mathbf{U}$ contains the volume-averaged density ρ, momentum ρu_i and total energy ρE. The inviscid flux tensor $\mathbf{F}$ is defined as

$$\mathbf{F}_i(\mathbf{U}) = \begin{bmatrix} \rho u_i \\ u_i \rho u_1 + \delta_{i1} p \\ u_i \rho u_2 + \delta_{i2} p \\ u_i \rho u_3 + \delta_{i3} p \\ u_i \rho E + u_i p \end{bmatrix} \tag{2.2}$$

and $\mathbf{G}$ is the viscous flux tensor

$$\mathbf{G}_i(\mathbf{U}) = -\begin{bmatrix} 0 \\ \tau_{i1} \\ \tau_{i2} \\ \tau_{i3} \\ u_k \tau_{ik} - q_i \end{bmatrix} \tag{2.3}$$

where τ_{ij} is the viscous stress tensor

$$\tau_{ij} = \mu \left[\left(\frac{\partial u_i}{\partial x_j} + \frac{\partial u_j}{\partial x_i} \right) - \frac{2}{3} \delta_{ij} \frac{\partial u_k}{\partial x_k} \right] \tag{2.4}$$

and q_i is the heat flux

$$q_i = -k \frac{\partial T}{\partial x_i} \tag{2.5}$$

where μ is the dynamic viscosity, k is the thermal conductivity, T is the temperature. We assume the fluid to be a perfect gas with the Prandtl number of $Pr = 0.72$ and a specific heats' ratio of $\gamma = c_p/c_v = 1.4$.

The above equations are nondimensionalized using the cord length c and the free stream values: the velocity U_0, the density ρ_0, and the temperature T_0. The pressure is nondimensionalized using $\rho_0 U_0^2$. The governing nondimensional flow parameters are the Reynolds number $Re = \rho_0 U_0 c/\mu_0$ and the Mach number $Ma = U_0/a_0$, where a_0 is the speed of sound based on T_0 and μ_0 is the viscosity in the free stream. Thermodynamic quantities are related through the nondimensional ideal-gas equation of state

$$p = \frac{1}{\gamma Ma^2} \rho T. \tag{2.6}$$

The nondimensional total energy per unit volume is

$$\rho E = \frac{1}{\gamma - 1} p + \frac{1}{2} \rho u_i u_i \ . \tag{2.7}$$

A power law is assumed for the temperature dependence of viscosity

$$\mu = \frac{1}{Re} T^{0.75} \tag{2.8}$$

and the thermal conductivity is

$$k = \frac{\mu}{(\gamma - 1) Ma^2 Pr} \ . \tag{2.9}$$

2.2. *Grid and boundary conditions*

The generation of suitable grids for LES of complex flows can be time-consuming and difficult. Contradictory requirements, such as adequate local resolution and minimum

number of grid points, can deteriorate the grid quality and adversely affect accuracy and numerical convergence properties. We use Cartesian grids, which facilitate automatic grid generation and adaptive local grid refinement by dyadic sub-partitioning. Cartesian grids also imply fewer computational operations per grid point than body-fitted or unstructured grids. On the other hand, geometric boundaries do not necessarily coincide with grid lines, so that boundary conditions have to be applied at the subcell level.

We use a conservative Immersed Boundary (IB) method for representing sharp interfaces between a fluid and a rigid body on Cartesian grids, see Refs. [12, 13]. A level-set technique is used for describing the interface geometry. The level-set function is the signed distance between each point in the computational domain and the immersed interface, which is positive within and negative outside of the fluid domain. The zero contour is the interface between the fluid and the obstacle. The intersection of the obstacle with the Cartesian grid produces a set of cells that are cut by the interface. The underlying finite-volume discretization is modified locally in these cut cells in such a way that it accounts only for the fluidic part of a cell. Required interface normals, face apertures and fluid-volume fractions of cut cells can be computed efficiently from the level-set function. The viscous stresses at the fluid-solid interface are approximated by linear differencing schemes. The interface pressure is obtained by solving the one-sided (symmetric) Riemann problem in the interface-normal direction.

As we operate on fluxes only, this cut-cell finite-volume method ensures mass, momentum, and energy conservation. Discrete conservation and a sharp representation of the fluid-solid interface render our method particularly suitable for LES of turbulent flows.

Characteristic boundary conditions of Poinsot and Lele [14] are applied at the far-field domain boundaries. At the downstream exit boundary, which will be subject to the passage of nonlinear fluid structures, a low value for the reflection parameter has been set. These boundary conditions avoid unphysical reflections that could strongly influence the flow in the vicinity of the airfoil.

2.3. *Finite volume discretization*

The Navier-Stokes equations are numerically solved on a grid that is too coarse to resolve all scales representing the turbulent fluid motion. The unavailable small-scale information, however, is crucial for the proper evolution of large-scale structures in the flow. Therefore, the effect on the resolved scales of their nonlinear interactions with the unresolved subgrid-scales (SGS) has to be represented by a SGS turbulence model.

Subgrid-scale models generally operate on flow scales that are marginally resolved by the underlying discretization scheme, i.e., the truncation error of common approximations for the convective terms can out-weigh the effect of even physically sound models. One can exploit this link by developing discretization methods where the truncation error itself functions as implicit SGS model. Approaches where SGS model and numerical discretization are merged are called implicit LES; refer to Ref. [15, 16] for an introduction.

Representing a full merger of discretization and SGS model, the Adaptive Local Deconvolution Method (ALDM) has shown to be a reliable, accurate, and efficient method for implicit LES of Navier-Stokes turbulence [17, 18]. The implicit SGS model provided by this discretization can be interpreted as a combination of eddy-viscosity and scale similarity modeling. Model parameters were determined by a spectral-space analysis of the effective eddy viscosity in isotropic turbulence in the Reynolds number's infinite limit by constraining the numerical dissipation to the physical SGS dissipation obtained from the analysis of nonlinear interactions in turbulence.

ALDM is used for discretizing the hyperbolic flux, whose discretization causes the SGS effects of interest, whereas standard second order centered differences are used for discretizing the viscous flux.

For comparative purposes other classic discretization schemes for the inviscid fluxes have been used in under-resolved DNS mode, i.e., without any explicit or implicit LES model. The other schemes used are 3rd and 5th order WENO with HLLC fluxes and 4th and 6th order central difference methods. These schemes were used because they are known to be either more dissipative (WENO schemes) or less dissipative (central difference schemes) than the ALDM discretization.

For time integration, the conditionally stable 3rd order Runge-Kutta method of Gottlieb and Shu [19] is used. This time-discretization scheme is total-variation diminishing (TVD) for $CFL \leq 1$, provided the underlying spatial discretization is TVD, whereas the linear stability bound is larger. As cut-cell methods can generate cells with a very small fluid volume fraction, a special treatment of such cells is necessary when excessively small time steps according to the CFL stability criterion are to be avoided. For increasing the computational efficiency, we use a conservative mixing procedure, where the conserved quantities in small cells are mixed with larger neighbors [12, 13]. During simulations, the time step size is adjusted dynamically according to the condition $CFL = 0.5$ based on the full cell size.

3. Results

3.1. *Computational Setup*

The geometry of the NACA-0012 airfoil at 5 degree of incidence and the computational grid are shown in Fig. 2. Several two dimensional Cartesian grids have been generated. Here we present only two different resolutions (coarsest and finest cases which will be referred to as "coarse" and "fine" grid). The coarse grid has around $240,000$ cells and the fine grid has around 1.6 million cells. For comparison, the baseline 2-D case of Jones *et al.* [6] used 1.6 million grid points. It should be noted that for the fine grid, even though the total number of cells is the same as in Jones *et al.* , the actual distribution of cells/points in the domain is quite different due to the distinct numerical approaches, i.e., Cartesian grid with IB versus generalized curvilinear coordinates.

To create 3-D grids the 2-D grids are extended in the spanwise direction using 32 points within the boundary layer, close to the airfoil and in the wake, reducing up to 4 points away from the airfoil where the flow is laminar to reduce the computational effort. The 3-D coarse grid has around 7.2 million cells and the fine grid has around 46.2 million cells. For comparison, the 3-D grid of Jones *et al.* [6] used 170.7 million grid points.

For each run, starting from a converged solution, the flow has been simulated for around 12 time units, c/U_0, where c is the airfoil cord length and U_0 the free stream velocity. The equations of motion have been nondimensionalized using c and U_0, therefore in the results shown $c = 1$ and $U_0 = 1$. Because of the low Mach number, the time step in the coarse grid had to be set to a low value of $\Delta t = 0.2 \times 10^{-4}$, which is a factor of 5 smaller than used by Jones *et al.* [6]. An even smaller time step is used for the fine grid.

3.2. *Numerical Simulations*

The project had been initiated during the first summer program [21] by performing 2-D low resolution simulations. During the current summer program, after several attempts to get a good agreement with the reference DNS, the original goal of using 1% of DNS

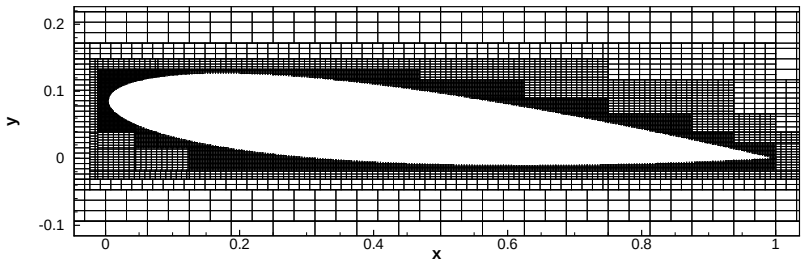

FIGURE 2. Grid around the airfoil, only every 5th line is shown (coarse grid).

resolution was abandoned and several runs with increasing resolution were performed. The challenges of obtaining good results at very low resolution come partially from the impossibility of stretching a cartesian grid at a curved IB. Several 2-D runs with the ALDM scheme and with increasing resolution have been made. It should be noted that, by design, ALDM provides a consistent SGS turbulence model for 3-D turbulence. In two dimensional or laminar flows ALDM does not provide a turbulence model but merely acts as a slightly dissipative, 2nd order accurate centered discretization. Therefore, the 2-D results presented should be considered as under-resolved DNS results, while the 3-D results should be considered as an implicit LES. 3-D simulations for the coarse and fine grid have been carried out only with the ALDM scheme.

Additionally, 2-D simulations with the fine grid and four different discretization schemes have been performed, in particular we have chosen two schemes that are more dissipative than ALDM (3rd and 5th order WENO schemes) and two that are less dissipative (4th and 6th order central difference schemes). All the simulations presented here are summarized in Tab. 1 for the 2-D simulations and Tab. 2 for the 3-D simulations

3.3. *Evaluation Metrics*

As a qualitative comparison the instantaneous spanwise vorticity field of the simulated flow is shown in Fig. 3 which can be compared with the results of Jones *et al.* [6]. The present 2-D and 3-D simulations capture well qualitative features observed in high resolution DNS, including the presence of a separated flow. In particular the characteristics of the laminar separation bubble described in Sec. 1 can be observed: laminar boundary layer, separated shear layer, break up of the shear layer, transition to turbulence, and turbulent reattachment. Only the vorticity fields for the coarse grid cases with the ALDM scheme are shown because all the other simulations look qualitatively similar.

As a principal quantitative metrics to evaluate our simulations we use quantities that are of paramount importance for the design of wings or blades: pressure coefficient, $C_p = (p - P)/\frac{1}{2}\rho U^2$, and skin friction coefficient, $C_f = \tau_w/\frac{1}{2}\rho U^2$ (where P is the free stream pressure, U is the free stream velocity, p is the pressure at the surface and τ_w is the wall shear stress). The pressure and friction coefficients from our simulations are compared with the corresponding data of Jones *et al.* [6] for their high resolution DNS case. All quantities are averaged in time for 10 time units. Also, for a numerical comparison of the location of the separation point x_s, the reattachment point x_p, and the bubble length l_b one should refer to Tab. 1 and Tab. 2 for the 2-D and 3-D cases, respectively. This quantitative information about the laminar separation bubble is extracted from the analysis of the skin friction coefficient plots (see Fig. 4(b) and Fig. 6(b)). In particular,

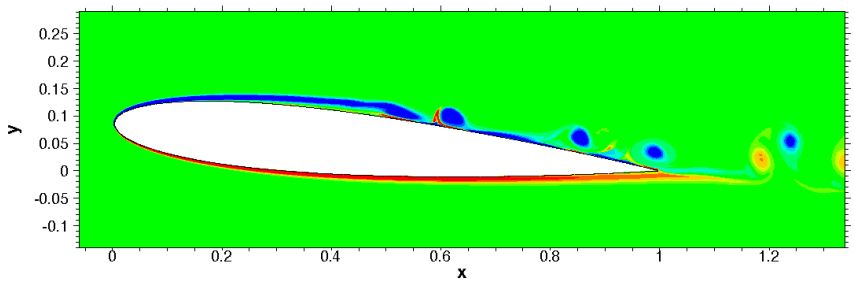

(a) Isocontours of vorticity for 2-D coarse grid simulation.

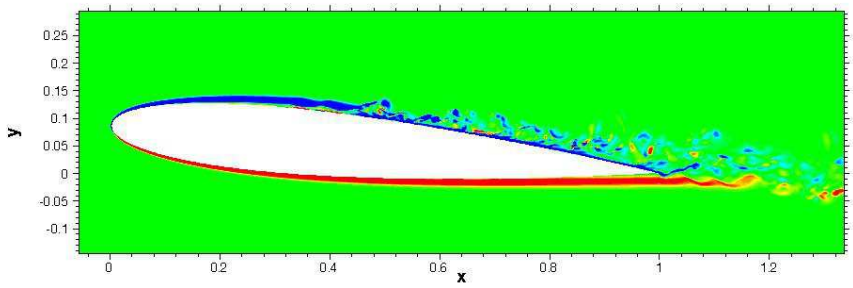

(b) Isocontours of vorticity for 3-D coarse grid simulation.

FIGURE 3. The spanwise vorticity field.

at the suction side the point where the skin friction becomes negative defines x_s and where the skin friction becomes positive again defines x_r.

3.3.1. *2-D simulations*

The comparison for the pressure coefficient (Fig. 4(a)) is quite good for all cases, especially on the pressure side of the airfoil; this is expected since on the pressure side the flow is fully laminar. The prediction of C_p on the suction side is not fully satisfactory for the cases with the ALDM scheme: the plateau formed due to the presence of the laminar separation bubble is captured, but the secondary peak at the end of the plateau is not. Substantially increasing the resolution, up to almost DNS resolution, improves the results. However it is not sufficient to reach perfect agreement with the DNS reference. The same trend can be observed looking at the skin friction coefficient (see Fig. 4(b)). There is overall agreement with the DNS reference, especially for the pressure side. Looking at the suction side all simulations predict accurately both separation and reattachment points. For the cases run with the ALDM scheme the magnitude and features of the secondary peak are not correctly captured even with the fine grid.

After a preliminary 3-D run (coarse grid with ALDM, see Fig. 6) it was noticed that the results were closer to the forced case of Jones *et al.* than to the unforced one. The forcing was added by Jones *et al.* to promote faster transition to turbulence in the 3-D simulations. This observation suggested that perhaps the IB procedure was generating some noise at the airfoil boundary and that these oscillations were acting as a forcing term promoting early transition to turbulence. In order to explore this idea additional runs with the fine grid were performed with schemes that are known to be more dissipative than ALDM, hoping that the additional numerical dissipation would damp out the oscil-

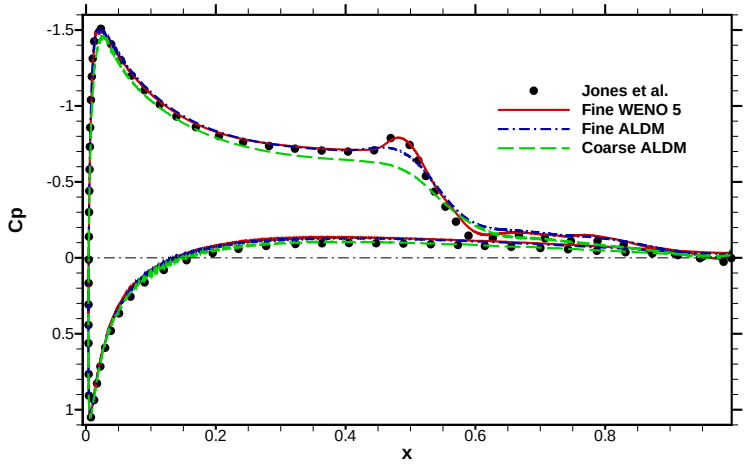

(a) Pressure coefficient comparison.

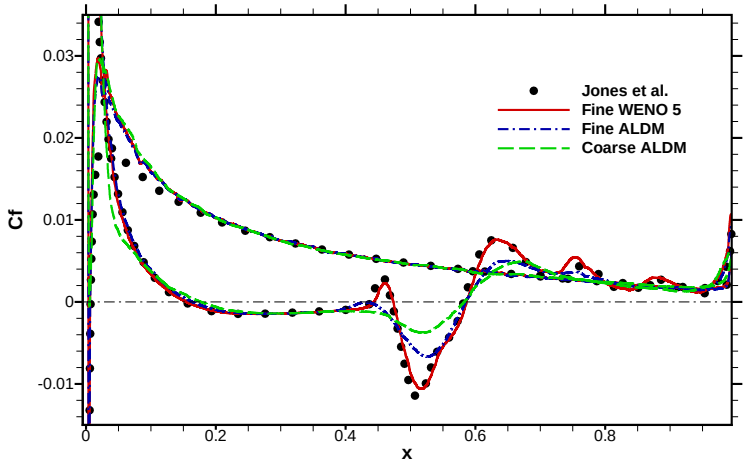

(b) Friction coefficient comparison.

FIGURE 4. 2-D Pressure and friction coefficients at the wall. DNS of Jones *et al.* [6] (black dots), 5th order WENO scheme with fine grid (solid red line), ALDM with fine grid (dashed dotted blue line), and ALDM with coarse grid (dashed green line).

lations originating from the IB method. The first run was made with a 3rd order WENO scheme. This brought an improvement in the results, notably the secondary peak after the bubble was now resolved, but the added numerical dissipation was excessive resulting in the shorter bubble length. The second run with a 5th order WENO scheme (denoted as WENO5 in the following) provided the right amount of numerical dissipation and all the features of the laminar separation bubble were fully captured as can be seen in Fig. 4.

In an attempt to further clarify the role of numerical dissipation in the difference be-

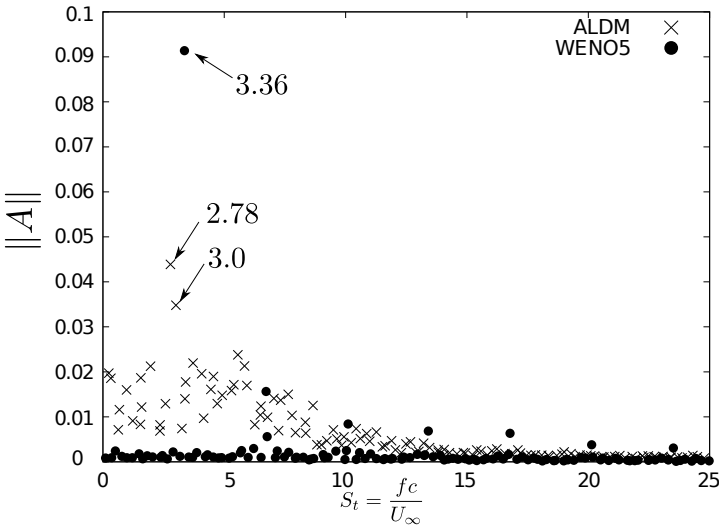

FIGURE 5. Results of the dynamic mode decomposition for WENO5 and ALDM simulations.

tween the results obtained with WENO5 and ALDM, two additional runs with the fine grid were made. This time 4th and 6th order central difference schemes were used. Both runs went unstable after a little more than one time unit, suggesting that these are under-resolved DNS.

Flow visualizations show an apparently identical flow evolution for the WENO5 and ALDM simulations. In order to identify and isolate the differences that lead to the discrepancy in the time averaged C_f and C_p distributions, we performed a Dynamic Mode Decomposition (DMD) for a sub-domain $0.3 \leq x \leq 0.85$ that fully encloses the region where flow-separation and vortex shedding takes place. DMD is a technique that allows for a modal analysis of any data sequence [22]. It is used here to identify modes and frequencies that express the dominant dynamic behavior captured in the simulated time series. Figure 5 shows the resulting frequencies and corresponding amplitudes. The difference between the two simulations is striking. For the WENO5 simulation, the dynamic behavior is fully governed by a single low-frequency dynamic mode with Strouhal number $St = 3.36$ and its higher harmonics. For the ALDM time series, DMD identifies two dominant low-frequency modes with $St = 3.0$ and $St = 2.78$, and a broad spectrum of less energetic modes that also contribute to the flow evolution. All relevant dynamic modes are very well resolved on the computational grid and have reached a saturated state.

We conclude that the pronounced secondary peaks of C_f and C_p in the WENO5 results are due to vortex shedding taking place at a constant streamwise coordinate and with constant frequency, which results in a single dynamic mode and its harmonics. The ALDM solution on the other hand is essentially dominated by two dynamic modes with slightly different frequencies. Though the shedded vortices have the same intensity as in the WENO5 run, this leads to a slight upstream-downstream oscillation of the vortex shedding location and a more smeared C_f and C_p distribution in the temporal average. We were unable to clearly identify the origin of the observed discrepancies between these two cases. Possible explanations are that the additional dynamic modes result from flow instabilities with small growth rates or from disturbances due to the geometry representation, which are suppressed if a more dissipative numerical method is used.

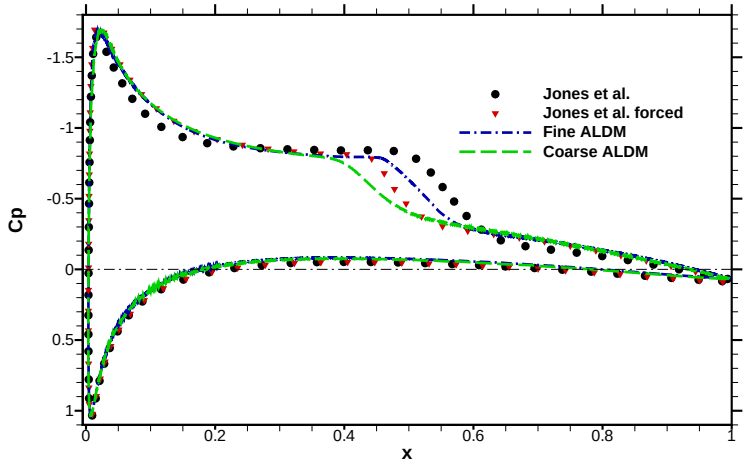

(a) Pressure coefficient comparison.

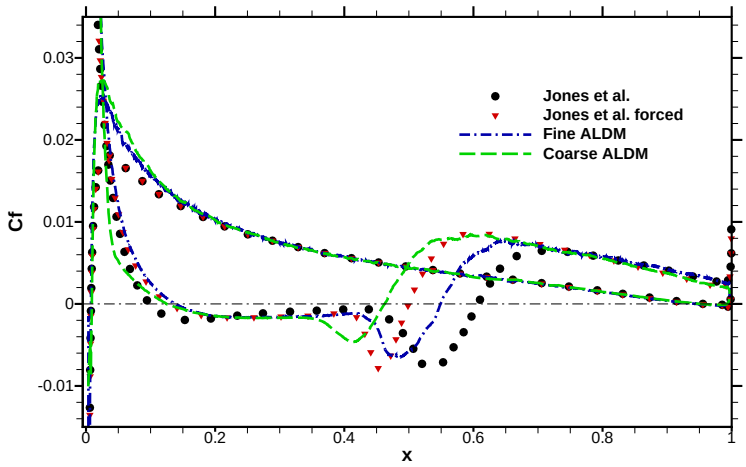

(b) Friction coefficient comparison.

FIGURE 6. 3-D Pressure and friction coefficients at the wall. DNS of Jones *et al.* [6] (black dots), DNS of Jones *et al.* [6] with forcing (red triangles), ALDM with fine grid (dashed dotted blue line), and ALDM with coarse grid (dashed green line).

3.3.2. *3-D simulations*

Only two 3-D simulations have been performed. Both 3-D simulations were performed with ALDM. The best agreement for the 2-D simulations was obtained with the 5th order WENO scheme, but it was decided to not perform a 3-D simulation with this scheme because it is known to have high levels of the numerical dissipation [23]. The high numerical dissipation would act as an uncontrolled implicit SGS model in case the simulation were to be performed without any explicit SGS model. On the other hand, if the

Simulation	Model	$N \times 10^6$	x_s	x_r	l_b
Jones *et al.* [6]	DNS	1.6	0.151	0.582	0.431
coarse	ALDM	0.24	0.177	0.583	0.406
fine	ALDM	1.6	0.164	0.585	0.421
fine	UDNS (WENO 3)	1.6	0.129	0.562	0.433
fine	UDNS (WENO 5)	1.6	0.155	0.586	0.431
fine	UDNS (CD 4)	1.6	-	-	-
fine	UDNS (CD 6)	1.6	-	-	-

TABLE 1. Summary of 2-D time averaged laminar separation bubble characteristics. N is the number of grid points, x_s the separation point, x_r the reattachment point and l_b the length of the bubble.

Simulation	Model	$N \times 10^6$	x_s	x_r	l_b
Jones *et al.* [6]	DNS	170.7	0.099	0.607	0.508
Jones *et al.* [6] forced	DNS	170.7	0.128	0.500	0.372
Almutairi *et al.* [20]	MTS	7.6	0.114	0.604	0.490
coarse	ALDM	7.2	0.125	0.462	0.337
fine	ALDM	46.2	0.138	0.549	0.411

TABLE 2. Summary of 3-D time averaged laminar separation bubble characteristics. N is the number of grid points, x_s the separation point, x_r the reattachment point and l_b the length of the bubble.

simulation were to be performed with an explicit SGS model the unknown numerical dissipation would contaminate the effects of the model [24].

For 3-D cases the pressure and the friction coefficients from both the forced and unforced DNS cases of Jones *et al.* are included for comparisons. The comparison for the pressure coefficient (Fig. 6(a)) is fairly good overall, although the bubble is visibly shorter compared to the unforced case for both grids. The more sensitive is the skin friction comparison shown in Fig. 6(b). Similarly to the 2-D case the pressure side is well reproduced. On the suction side, the separation point is fairly well captured, although for both grids it agrees better with the forced case of Jones *et al.* . The reattachment point varies substantially between the coarse and fine grid cases and the bubble in both cases is significantly shorter than in the benchmark DNS. We may speculate that the noise from the immersed boundary procedure promotes early transition to turbulence and consequently early reattachment. With the finer grid the forcing is weaker and the IB solution approximates better the reference DNS data.

4. Conclusions

We have initiated a project to apply and evaluate LES techniques to simulate separated flows with *resolution reduced drastically from that used in DNS and typical LES performed for such problems*, the reduction target being a factor of at least 100. As the first step toward this goal we have adapted the numerical code INCA developed at TUM that uses immersed boundary method to simulate a flow around a NACA-0012 airfoil for which a detailed DNS database is available [6]. 2-D and 3-D simulations at

low resolution, around the reduction target have been performed, and at this resolution our simulations reproduce qualitative features of the flow such as the structure of the vorticity field and the presence of a separation. We also obtain a fairly good quantitative prediction for the pressure coefficient and the location of the primary separation point.

For a better quantitative agreement a DNS-like resolution is needed and any computational savings with respect to actual DNS can only be obtained by decreasing the resolution in the homogenous (spanwise) direction. The reattachment point in the 3-D case is very sensitive to the resolution. We speculate that this behavior can be attributed to the noise coming from the IB procedure rather than from not having the correct SGS dissipation. This is supported by the results of 2-D simulations, where a dissipative code provided an excellent agreement with the DNS benchmark. A DMD analysis revealed that the flow dynamics predicted by the dissipative method is fully captured with a single dynamic mode and its harmonics. Hence, vortex shedding takes place at a constant streamwise coordinate, leading to pronounced secondary peaks of C_f and C_p in agreement with the DNS. With a less dissipative method, however, the vortex shedding is essentially dominated by two different low-frequency dynamic modes, which leads to a slight upstream-downstream oscillation of the vortex shedding location and a smeared C_f and C_p distribution in the temporal average.

A separate conclusion regarding LES for such problems in the framework of IB methods is that because of difficulties in resolving geometry of a curved wall with a Cartesian grid the IB methods are more appropriate for a high resolution/fidelity LES rather than for very coarse LES which can take an advantage of high-aspect-ratio body fitted grids to resolve the wall region.

Acknowledgments

Two co-authors (GC and JAD) gratefully acknowledge support for this project provided through the second SFB/TRR 40 Summer Program and the hospitality of faculty and staff of Lehrstuhl für Aerodynamik und Strömungsmechanik, Technische Universität München. The first two co-authors have been also supported by a NSF grant (CBET-1233160). Finally we would like to thank Dr. Sandham for providing the DNS results.

References

[1] HU, H., YANG, Z. AND IGARASHI, H. (2007). Aerodynamic hysteresis of a low-Reynolds-number airfoil. *J. Aircraft*, **44**, 2083–2086.

[2] HAIN, R., KAEHLER, C. J. AND RADESPIEL, R. (2000). Dynamics of laminar separation bubbles at low-Reynolds-number aerofoils. *J. Fluid Mech.*, **630**, 129–153.

[3] SPEDDING, G. R. AND MCARTHUR, J. (2010). Span efficiencies of wings at low Reynolds numbers. *J. Aircraft*, **47**, 120–128.

[4] LIN, J. C. M. AND PAULEY, L. L. (1996). Low-Reynolds-number separation on an airfoil. *AIAA J.*, **34**, 1570–1577.

[5] ALAM, M. AND SANDHAM, N. D. (2000). Direct numerical simulation of 'short' laminar separation bubbles with turbulent reattachment. *J. Fluid Mech.*, **410**, 1–28.

[6] JONES, L. E., SANDBERG, R. D. AND SANDHAM, N. D. (2008). Direct numerical simulations of forced and unforced separation bubbles on an airfoil of incidence. *J. Fluid Mech.*, **602**, 175–207.

[7] JONES, L. E., SANDBERG, R. D. AND SANDHAM, N. D. (2010). Stability and receptivity characteristics of a laminar separation bubble on an airfoil. *J. Fluid Mech.*, **648**, 257–296.

[8] SPALART, P. R. AND STRELETS, M. K. (2000). Mechanisms of transition and heat transfer in a separation bubble. *J. Fluid Mech.*, **403**, 329–349.

[9] WILSON, P. G. AND PAULEY, L. L. (1998). Two- and three-dimensional large-eddy simulations of a transitional separation bubble. *Phys. Fluids*, **10**, 2932–2940.

[10] YANG, Z. AND VOKE, P. R. (2001). Large-eddy simulation of boundary-layer separation and transition at a change of surface curvature. *J. Fluid Mech.*, **439**, 305–333.

[11] EISENBACH, S. AND FRIEDRICH, R. (2008). Large-eddy simulation of flow separation on an airfoil at a high angle of attack and $Re = 10^5$ using Cartesian grids. *Theor. Comput. Fluid Dyn.*, **22**, 213–225.

[12] MEYER, M., DEVESA, A., HICKEL, S., HU, X. Y. AND ADAMS, N. A. (2010). A conservative immersed interface method for large-eddy simulation of incompressible flows. *J. Comput. Phys.*, **229**, 6300–6317.

[13] GRILLI, M., HICKEL, S., HU, X. Y. AND ADAMS, N. A. (2009). Conservative immersed boundary method for compressible flows. *Academy Colloquium on Immersed boundary methods: current status and future research directions*, Amsterdam, The Netherlands.

[14] POINSOT, T. J. AND LELE, S. K. (1992). Boundary Conditions for Direct Simulations of Compressible Viscous Flows. *J. Comput. Phys.*, **101**, 104–129.

[15] GRINSTEIN, F., MARGOLIN, L. AND RIDER, W. (2007). *Implicit Large Eddy Simulation: Computing Turbulent Flow Dynamics*, Cambridge, UK: Cambridge University Press.

[16] GARNIER, E., ADAMS, N. AND SAGAUT, P. (2009). *Large eddy simulation for compressible flows*, Springer.

[17] HICKEL, S., ADAMS, N. A. AND DOMARADZKI, J. A. (2006). An adaptive local deconvolution method for implicit LES. *J. of Comput. Phys.* **213**, 413–436.

[18] HICKEL, S. AND LARSSON, J. (2008). An adaptive local deconvolution model for compressible turbulence. *Proceedings of the 2008 Summer Program, Center for Turbulence Research, Stanford University*, 85–96.

[19] GOTTLIEB, S. AND SHU C.-W. (1998). Total variation diminishing Runge-Kutta schemes. *Math. Comput.*, **67**, 73–85.

[20] ALMUTAIRI, J. H., JONES, L. E. AND SANDHAM, N. D (2010). Intermittent bursting of a laminar separation bubble on an airfoil. *AIAA J.*, **48**, 414–426.

[21] CASTIGLIONI, G., DOMARADZKI, J. A., GRILLI, M. AND HICKEL, S. (2011). Numerical modeling of separated flows at moderate Reynolds numbers appropriate for turbine blades and unmanned aero vehicles. *SFB/TRR 40 – Proceedings of the Summer Program 2011*, 67–76

[22] SCHMID, P. J. (2010). Dynamic mode decomposition of numerical and experimental data. *J. Fluid Mech.*, **656**, 5–28.

[23] TAIEB, D., RIBERT, G. AND HADJADJ, A. (2010). Numerical simulations of shock focusing over concave surfaces. *AIAA J.*, **48**, 1739–1747.

[24] CADIEUX, F., DOMARADZKI, J. A., SAYADI, T. AND BOSE, T. (2013). DNS and LES of Laminar Separation Bubbles at Moderate Reynolds Numbers. *ASME J. Fluids Eng.*, in press.